to both minimal and *IL12* gene promoters, thus impairing their transcription (Fig. 6, B to E, and fig. S20C). Accordingly, β-catenin deficiency impeded MUC2-mediated inhibition of LPS-induced IL-12 but not IL-10 transcription and/or secretion, whereas β-catenin overexpression dampened TNF-induced NF-κB–driven transcription (Fig. 6, F and G, and fig. S20, D to F). Consistent with these data, galectin-3–expressing DCs from PPs contained abundant β-catenin in addition to activated AKT and inactive GSK-3β (Fig. 6H).

Besides AKT, Dectin-1 phosphorylates SYK, which activates NF-κB through a pathway mitigated by FcγRIIB via SH2 domain–containing inositol 5-phosphatase-1 (SHIP-1) (*22*, *26*). SYK also activates cAMP responsive element binding protein (CREB), a calcium-dependent IL-10–inducing protein that removes the co-activator CREB-binding protein (CBP) from DNA-bound NF-κB (*27*, *28*). Besides triggering SYK and SHIP-1 phosphorylation, MUC2 alone or combined with LPS decreased NF-κB p65 but not p50 nuclear translocation and increased galectin-dependent calcium fluxes, phosphorylation of CREB-targeting AKT, ERK1/2 and p38 kinases, phosphorylation and nuclear translocation of CREB, binding of CREB to *IL10* and *IL12* promoters, and loss of CBP from the *IL12* promoter (figs. S20G and S21, A to G). Thus, similar to hyperglycosylated IgG Abs used to treat autoimmune disorders (*22*), MUC2 may recruit SHIP-1 via FcγRIIB to constrain proinflammatory NF-κB but not tolerogenic CREB signals emanating from Dectin-1 and SYK. In addition to inducing IL-10, CREB may cooperate with Dectin-1–induced β-catenin to inhibit NF-κB–dependent IL-12 production.

Conclusions

We have shown here that MUC2 enhances gut homeostasis and oral tolerance by conditioning DCs and IECs. Antigen-sampling DCs assemble galectin-3, Dectin-1, and FcγRIIB to acquire MUC2 across IECs and possibly from GCs (fig. S22A). This MUC2 receptor complex suppresses inflammatory but not tolerogenic DC responses by inhibiting NF-κB via β-catenin (fig. S22B). How DCs tune down these signals during infection remains unclear, but pathogen-induced perturbations of MUC2 glycosylation and polymerization patterns may be involved (*1*). A full understanding of the immunoregulatory function of MUC2 could help to devise better vaccines and treatments against infections and food allergies and to unravel how alterations of MUC2 and its receptors aggravate inflammatory bowel disease (*1*, *20*), thus leading to safer therapies against this disorder.

References and Notes

1. M. E. Johansson, J. M. Larsson, G. C. Hansson, *Proc. Natl. Acad. Sci. U.S.A.* **108** (suppl. 1), 4659–4665 (2011).
2. J. L. Coombes, F. Powrie, *Nat. Rev. Immunol.* **8**, 435–446 (2008).
3. A. Cerutti, K. Chen, A. Chorny, *Annu. Rev. Immunol.* **29**, 273–293 (2011).
4. M. Rescigno *et al.*, *Nat. Immunol.* **2**, 361–367 (2001).
5. J. H. Niess *et al.*, *Science* **307**, 254–258 (2005).
6. J. Farache *et al.*, *Immunity* **38**, 581–595 (2013).
7. J. L. Coombes *et al.*, *J. Exp. Med.* **204**, 1757–1764 (2007).
8. M. Bogunovic *et al.*, *Immunity* **31**, 513–525 (2009).
9. J. R. McDole *et al.*, *Nature* **483**, 345–349 (2012).
10. C. I. Yu *et al.*, *Immunity* **38**, 818–830 (2013).
11. D. Mucida *et al.*, *Science* **317**, 256–260 (2007).
12. A. Velcich *et al.*, *Science* **295**, 1726–1729 (2002).
13. I. D. Iliev, E. Mileti, G. Matteoli, M. Chieppa, M. Rescigno, *Mucosal Immunol.* **2**, 340–350 (2009).
14. M. Rimoldi *et al.*, *Nat. Immunol.* **6**, 507–514 (2005).
15. S. Vaishnava *et al.*, *Science* **334**, 255–258 (2011).
16. A. Esteban *et al.*, *Proc. Natl. Acad. Sci. U.S.A.* **108**, 14270–14275 (2011).
17. S. Dillon *et al.*, *J. Clin. Invest.* **116**, 916–928 (2006).
18. J. M. Ilarregui *et al.*, *Nat. Immunol.* **10**, 981–991 (2009).
19. Y. Zhou *et al.*, *Nat. Med.* **16**, 1128–1133 (2010).
20. I. D. Iliev *et al.*, *Science* **336**, 1314–1317 (2012).
21. G. A. Rabinovich, M. A. Toscano, *Nat. Rev. Immunol.* **9**, 338–352 (2009).
22. C. M. Karsten *et al.*, *Nat. Med.* **18**, 1401–1406 (2012).
23. K. M. Dennehy, J. A. Willment, D. L. Williams, G. D. Brown, *Eur. J. Immunol.* **39**, 1379–1386 (2009).
24. S. Manicassamy *et al.*, *Science* **329**, 849–853 (2010).
25. J. Deng *et al.*, *Cancer Cell* **2**, 323–334 (2002).
26. D. Strasser *et al.*, *Immunity* **36**, 32–42 (2012).
27. E. K. Kelly, L. Wang, L. B. Ivashkiv, *J. Immunol.* **184**, 5545–5552 (2010).
28. A. Y. Wen, K. M. Sakamoto, L. S. Miller, *J. Immunol.* **185**, 6413–6419 (2010).

Acknowledgments: This study was supported by the National Institute of Allergy and Infectious Diseases, NIH (AI61093, AI57653, AI95613, AI96187 and AI74378 to A.C. and AI073899, DK072201 and AI095245 to J.M.B.) and by Redes Temáticas de Investigación Cooperativa en Salud/Fondo Europeo de Desarrollo Regional (RD12/0036/0054 to A.B). pRSETb-mRFP used for red bacteria is under a materials transfer agreement with R. Y. Tsien at the University of California, San Francisco, and Howard Hughes Medical Institute. The data presented in this manuscript are tabulated in the main paper and the supplementary materials.

Supplementary Materials

www.sciencemag.org/content/342/6157/447/suppl/DC1
Materials and Methods
Acknowledgments
Figs. S1 to S22
Tables S1 to S8
References (*29*–*37*)
Movies S1 and S2

18 March 2013; accepted 5 September 2013
Published online 26 September 2013;
10.1126/science.1237910

Observation of Floquet-Bloch States on the Surface of a Topological Insulator

Y. H. Wang,* H. Steinberg, P. Jarillo-Herrero, N. Gedik†

The unique electronic properties of the surface electrons in a topological insulator are protected by time-reversal symmetry. Circularly polarized light naturally breaks time-reversal symmetry, which may lead to an exotic surface quantum Hall state. Using time- and angle-resolved photoemission spectroscopy, we show that an intense ultrashort midinfrared pulse with energy below the bulk band gap hybridizes with the surface Dirac fermions of a topological insulator to form Floquet-Bloch bands. These photon-dressed surface bands exhibit polarization-dependent band gaps at avoided crossings. Circularly polarized photons induce an additional gap at the Dirac point, which is a signature of broken time-reversal symmetry on the surface. These observations establish the Floquet-Bloch bands in solids and pave the way for optical manipulation of topological quantum states of matter.

Three-dimensional topological insulators (TIs) host an exotic surface state that obeys the Dirac equation and exhibit spin-momentum locking. The gapless surface states are protected by time-reversal symmetry (TRS), the breaking of which is predicted to lead to many exotic phenomena (*1*–*3*). Doping TIs with magnetic impurities breaks TRS on the surface (*4*–*7*), but it also introduces disorder (*8*); the coherent interaction between light and matter is a promising alternative route toward such a broken symmetry phase (*9*–*12*). This coherent effect is seen in atoms and molecules as hybridized states distinctive in their energy spectra (*13*, *14*) and in photonic systems as Floquet states (*15*). In solid-state systems, the photon-dressed bands lead to a periodic band structure in both energy and momentum called Floquet-Bloch states (*16*). In the case of TIs, an additional effect is expected to take place when circularly polarized light is coupled with the surface states: TRS will be spontaneously broken and the surface Dirac cone becomes gapped (*9*, *17*).

Floquet theorem states that a Hamiltonian periodic in time has quasistatic eigenstates that are evenly spaced by the drive photon energy (*18*).

Department of Physics, Massachusetts Institute of Technology, Cambridge, MA 02139, USA.

*Present address: Department of Physics and Applied Physics, Stanford University, Stanford, CA 94305, USA.
†Corresponding author. E-mail: gedik@mit.edu

These so-called Floquet states can be regarded as a time analog of Bloch states, which are the eigenstates of a Hamiltonian periodic in space (*19*). Combining the two situations, a periodic excitation on a crystalline lattice induces Floquet-Bloch bands that repeat in both momentum and energy. Just as different Bloch bands hybridize and develop band gaps at the crossing points (*19*), the crossing points between different orders (n) of the Floquet-Bloch bands open dynamic gaps (*16*, *20*). Although conventional optical spectroscopy (*21*–*23*) and photoemission spectroscopy (*24*, *25*) have shown many coherent phenomena under intense radiation, a technique that can probe the states in an energy-momentum–resolved manner while applying a strong photoexcitation is needed to image the Floquet-Bloch states and the photo-induced band gaps on the surface of a TI.

Time- and- angle-resolved photoemission spectroscopy (TrARPES) is a powerful technique capable of resolving such photo-induced band gaps (*26*–*28*). When the photon energy of the laser that excites the sample is below the bulk band gap (typically less than 300 meV), the coherent interaction between light and the TI surface states is the dominant effect (*10*, *11*). To achieve this regime, we used polarized photons at midinfrared (MIR) wavelengths to investigate the photon-dressed surface states in TIs.

We used a time-of-flight spectrometer to simultaneously acquire the complete surface band structure of Bi_2Se_3 without changing the sample or

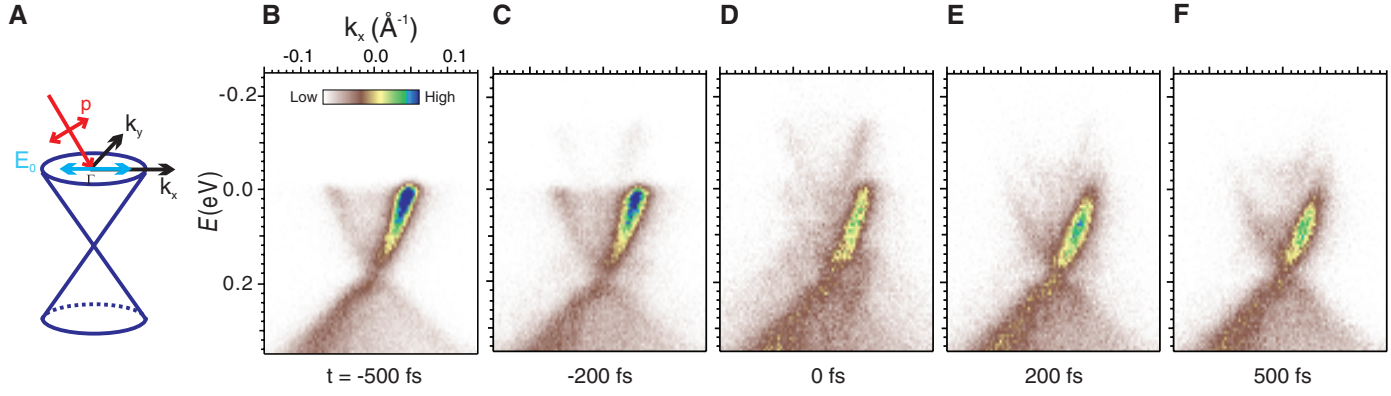

Fig. 1. Angle-resolved photoemission spectra (APRES) of Bi_2Se_3. (**A**) A sketch of the experimental geometry for the p-polarized case. k_x is defined to be the in-plane electron momentum parallel to the pump scattering plane. (**B** to **F**) ARPES data for several pump-probe time delays t (values indicated in the figure) under strong linearly polarized mid-infrared (MIR) excitation of wavelength λ = 10 μm.

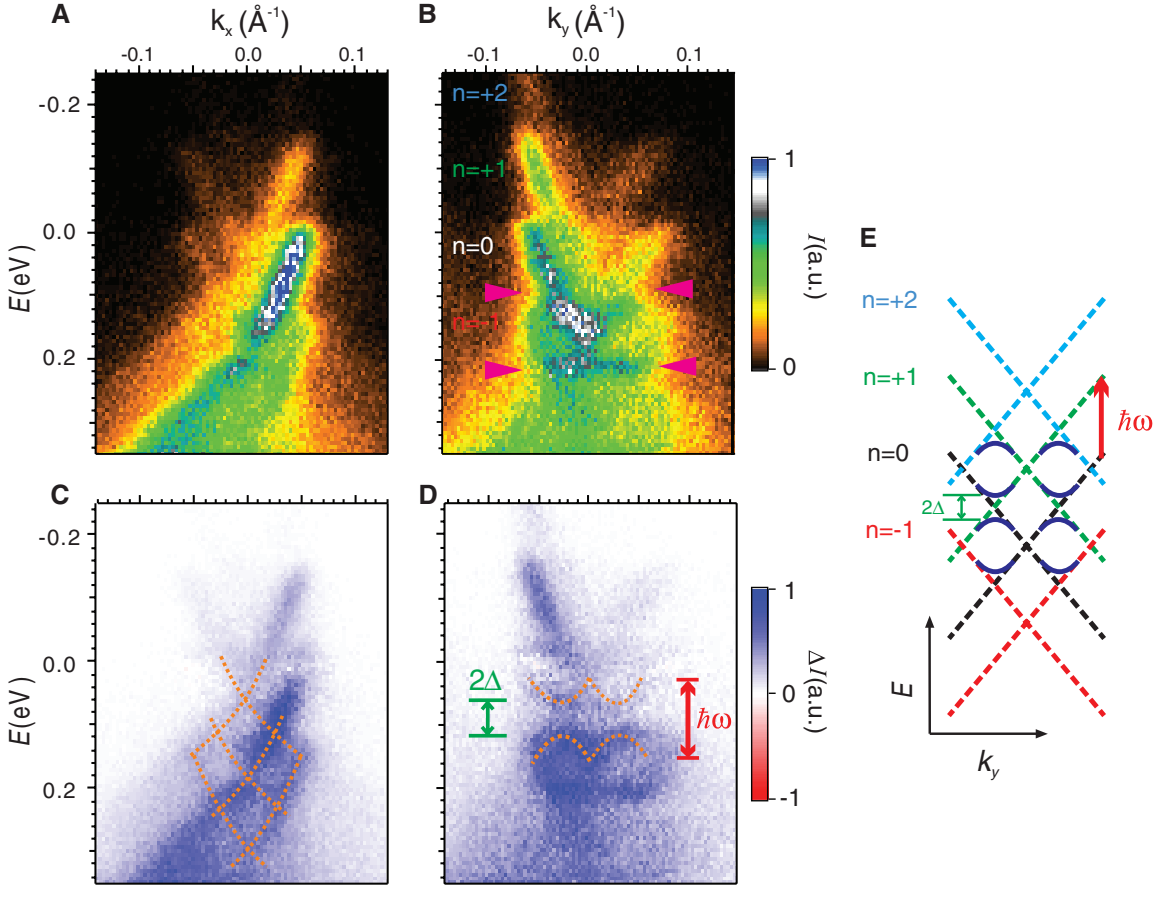

Fig. 2. ARPES spectra at 0 fs time delay under linearly polarized MIR excitation. (**A**) and (**B**) show the energy-momentum spectra through Γ along the k_x and k_y directions, respectively. (**C**) and (**D**) are the same spectra after subtracting the spectra at t = –500 fs (*35*). Dashed orange lines are guides to the eye. (**E**) Sketch of the side bands of different order as induced by the midinfrared excitation. Avoided crossing occurs along k_y, leading to a pattern of ∞ around the Dirac point. ω is the drive photon frequency, and Δ is the half gap at the avoided crossings.

the detector orientation in a pump-probe scheme (*28*, *29*). The MIR pump pulses are generated from a commercial optical parametric amplifier pumped by a Titanium:Sapphire amplifier. The output pulses are tunable in wavelength from 4 μm to 17 μm with 1 μJ peak energy. The MIR pulses are focused to a 300-μm diameter spot [full width at half maximum (FWHM)] on the single-crystal Bi_2Se_3 sample at an angle of 45°. The pulsewidth is estimated to be 250 fs (FWHM) from the rising edge of the momentum-integrated time spectrum (fig. S1D). We estimated the amplitude of the electric field to be $E_0 = 2.5(\pm1) \times 10^7$ V/m on the surface of the sample after taking into account the loss through the optics, the geometric effect, and the Fresnel reflection (*30*) at the vacuum-sample interface (*31*). The polarization of the MIR pulse is adjusted by a quarter wave-plate. Figure 1A illustrates the p-polarized case in which the electric field of light is in the plane of incidence. The component of the surface electron momentum in the plane of incidence is defined as k_x.

Figure 1, B to F, shows energy-momentum spectra of Bi_2Se_3 obtained at several time delays t after the intense linearly polarized MIR excitation. At $t = -500$ fs, the probe ultraviolet (UV) pulse is ahead of the MIR pulse and the band structure is similar to that of an unperturbed system (Fig. 1B) (*28*). The asymmetry in the spectral intensity about zero momentum Γ is due to the coupling between the linearly polarized UV pulse and the spin-orbit texture of the surface states of TI (*29*). When the two pulses start to overlap in time ($t = -200$ fs), replicas of the surface Dirac cone appear above and below the original band (Fig. 1C). The energy difference between the bands equals exactly the pump photon energy of $\hbar\omega = 120$ meV, where ħ is the reduced Planck constant and ω is the angular frequency of light. The intensity of such side bands becomes stronger, whereas the original band gets weaker when the pump and probe pulses are completely overlapped at $t = 0$ (Fig. 1D). When the side bands become weaker again at 200 fs (Fig. 1E), the spectral intensity still above the Fermi level occupies the higher energy states of the original surface and bulk bands rather than the side bands. This suggests the onset of a thermally excited carrier population, as has been observed previously with 1.5-eV photoexcitations (*26*, *28*). This excited population is still present at 500 fs (Fig. 1F), consistent with the observed photoexcited carrier cooling time in this material (*26*, *28*). The fact that the side bands are only present during the time duration of the pump pulse suggests that it is a consequence of the coherent interaction between the MIR photons and the electron system. In a TrARPES experiment, a strong IR field may also generate band replicas through laser-assisted photoemission (LAPE) (*24*, *25*). Because this effect is caused by the absorption of pump photons by the near-free electrons in the final states of photoemission, the LAPE bands do not open band gaps where they cross, and their intensity is at a minimum in the direction perpendicular to the light polarization, which is inconsistent with our findings (*31*).

To see how the photon-dressed bands change with respect to the polarization of light and whether there are band gaps, we compared the energy momentum spectra taken at $t = 0$ fs along the directions parallel and perpendicular to the electric field of the linearly polarized pump (Fig. 2). Compared with the side bands along k_x (Fig. 2A), the side bands in the k_y direction show a higher order ($n = +2$) more clearly (Fig. 2B). More important, the bands are much stronger and show features that deviate from a mere stacking of Dirac cones at energies close to the $n = 0$ Dirac point ($0.15\ \text{eV} < E < 0.3$ eV). The otherwise linearly dispersing $n = 0$ cone becomes discontinuous and distorted at $E = 0.1$ eV and 0.22 eV (Fig. 2B, pink triangles).

To better visualize these features, we subtracted the spectrum taken at $t = -500$ fs from the spectrum at $t = 0$ fs, which includes the spectral contribution from the unperturbed surface bands due to the finite pulse width (*31*). The difference spectrum along k_y (Fig. 2D) shows a pattern resembling an ∞ sign centered at the $n = 0$

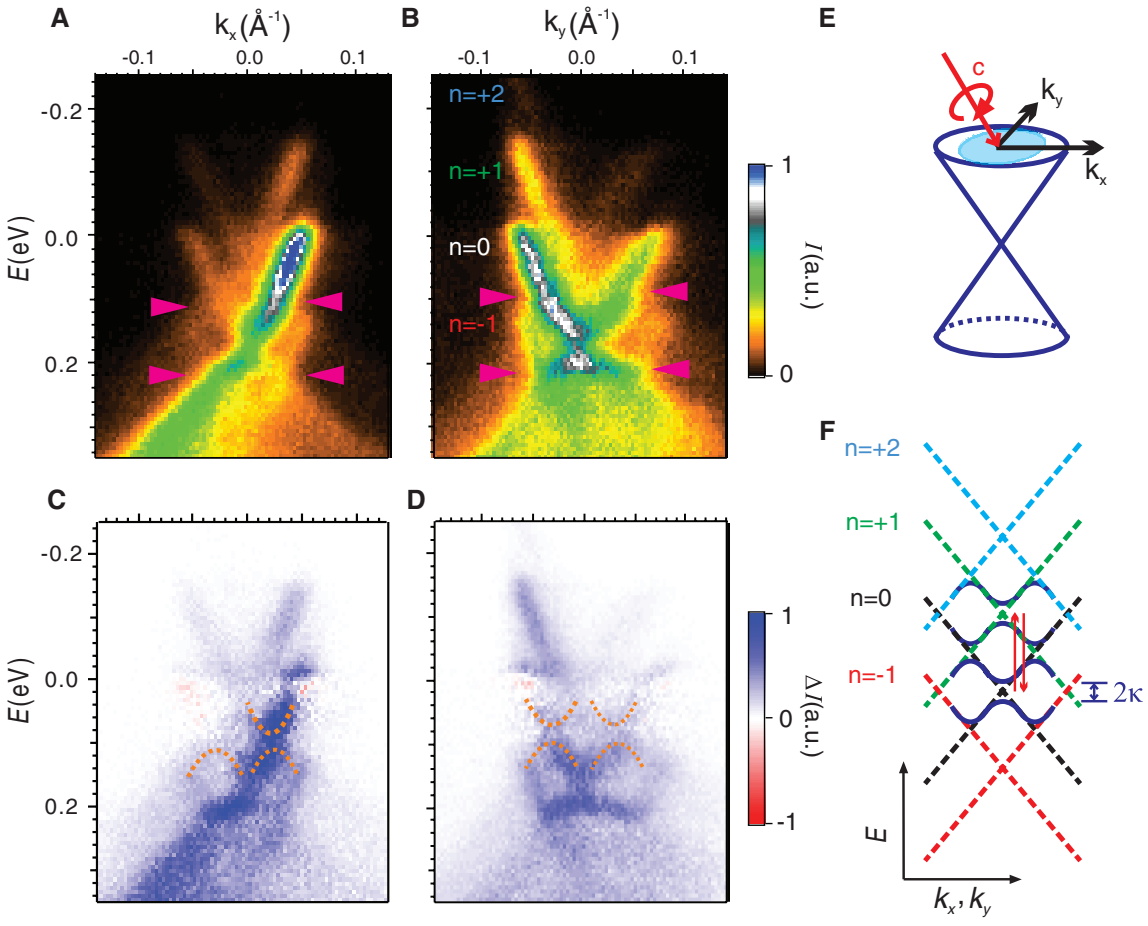

Fig. 3. ARPES spectra at 0 fs time delay under circularly polarized MIR excitation. (**A** to **D**) are analogous to the corresponding panels in Fig. 2. (**E**) The projection of the electric field on the surface plane (light blue) is elliptical, and the avoided crossing appears along both directions. The chirality allows emitting and absorbing a photon to open a band gap at the Dirac point as sketched in the side-band diagram in (**F**). κ is half of the band gap at the Dirac point.

Dirac point. There is a replica of this ∞ pattern at one pump photon energy (120 meV) above the one around $n = 0$ Dirac point, suggesting that this is a coherent feature on the photo-induced bands. $E = 0.1$ eV is the middle point of these two ∞, suggesting that the kinks in the raw spectrum (Fig. 2B) correspond to opening of band gaps. These features are in contrast with the difference spectrum in the k_x direction, where the pattern is simply composed of three Dirac cones shifted by $\hbar\omega$ (Fig. 2C). This momentum-dependent feature is consistent with the prediction of photon-dressed Dirac bands in graphene under linearly polarized light (*32*–*34*), where Floquet-Bloch bands open band gaps along the direction perpendicular to the electric field, whereas the bands with momentum parallel to the field remain gapless.

For an ideal Dirac cone (Fig. 2E), the avoided crossing between adjacent orders is centered at momenta $\pm\omega/2v$, where v is the Fermi velocity of the surface states. In our case, we can see in the difference spectra the crossing of bands at $k_x \sim \pm 0.03$ Å^{-1} (Fig. 2C), whereas the band gaps appear at similar values of k_y (Fig. 2D). This is slightly bigger than the expected value of $\omega/2v = 0.02$ Å^{-1} [using $\hbar\omega = 120$ meV and $\hbar v = 3$ eVÅ (Fig. 1A)], likely resulting from the reduced velocity of bands below the Dirac point (Fig. 1). At $k_y = \pm 0.06$ Å^{-1}, where $n = \pm 1$ cross, there is no resolvable gap (Fig. 2D). Therefore, the ∞ pattern around the $n = 0$ Dirac point is a result of the crossings and avoided crossings between $n = 0$ and $n = \pm 1$ (Fig. 2, D and E). The energy distribution curve (fig. S1A) through the avoided crossing shows a 2Δ value of 62 meV. Along with the crossings and avoided crossings between different orders, the gap size is consistent with the theory of photon-dressed Dirac systems based on the Floquet picture (*31*–*34*).

Having shown that linearly polarized MIR photons couple with the surface states into Floquet-Bloch bands, we investigated how these bands change when the photons become circularly polarized. Unlike the bands under linearly polarized light, the spectrum under circularly polarized light shows avoided crossings at ~±0.03 Å^{-1} along both k_x and k_y (Fig. 3, A to D). Spectral cuts along other in-plane directions through Γ (fig. S3C) further show that the dynamical gap does not close for any direction. This is consistent with the Floquet-Bloch bands generated by the coupling between circularly polarized in-plane electric field and the surface states (Fig. 3E).

Knowing that the surface electrons and the rotating electric field of the circularly polarized MIR pulse are coupled, we examined the Dirac point of the induced Floquet-Bloch bands for signatures of TRS breaking (Fig. 3F). The spectral weight above and below the Dirac point increases at $t = 0$ for both polarizations (Figs. 2, C and D, and 3, C and D). To be able to resolve any gap around the Dirac point, we converted the intensity spectra for both polarizations (Figs. 2B and 3B) into energy distribution curves (EDCs) by integrating the spectra over a small momentum window (0.005 Å^{-1}) at each momentum point along k_y (Fig. 4). The EDCs show that only the spectrum obtained under circularly polarized excitations opens a band gap at the Dirac point (Fig. 4A), whereas such a gap is absent in the curves taken under linearly polarized light (Fig. 4B). The EDC through the Γ point under circularly polarized light clearly show two peaks at the Dirac point (Fig. 4C, blue). [The small hump in the EDC under linearly polarized excitation (Fig. 4C, red) is a result of the finite momentum resolution of our spectrometer (~0.005 Å^{-1}) and is also visible in the EDC of unperturbed spectrum (Fig. 4C, black).] This result is similarly observed in the difference spectrum between the two polarizations as negative spectral weight at the Dirac point (fig. S4A). By fitting the EDC through the Γ point in Fig. 4A, we obtained the band gap $2\kappa = 53$ meV (fig. S1B). Using the 2Δ value we obtained from the dynamic gap (*31*), we found that the Dirac gap is consistent with the gap resulting from the two-photon process (absorbing and emitting a photon) that is only allowed under circular polarization that breaks TRS (*9*, *34*).

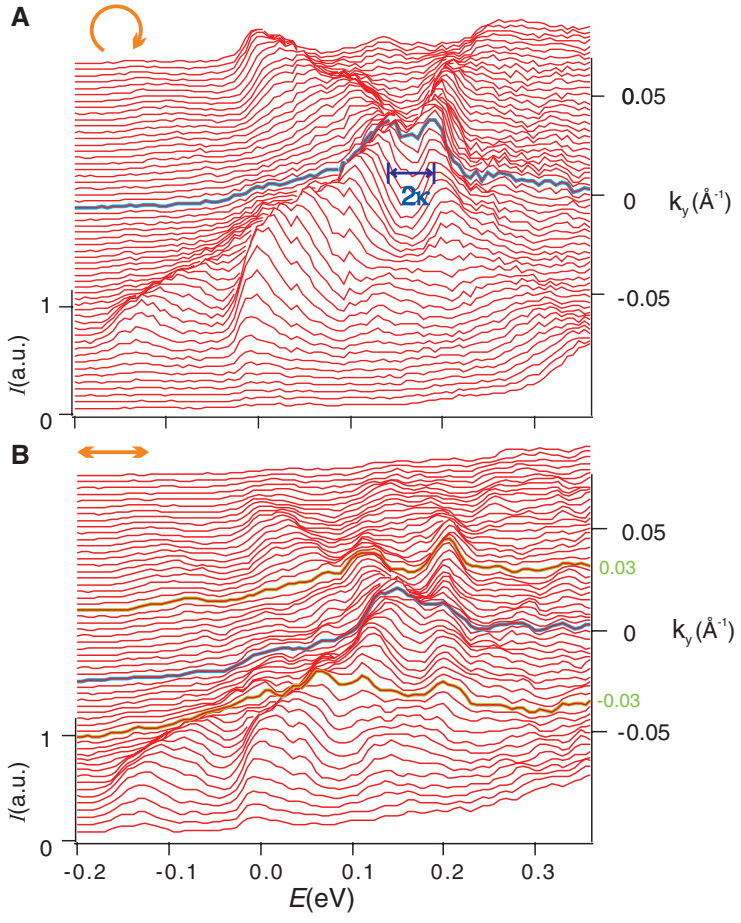

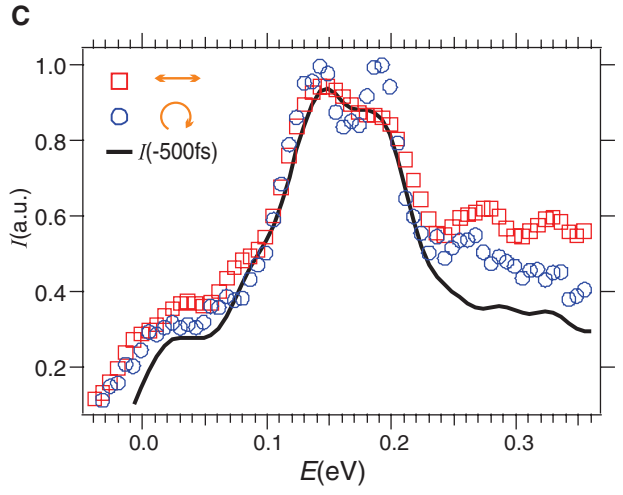

Fig. 4. Band gap at the Dirac point induced by circularly polarized MIR pulse. (**A**) and (**B**) show the energy distribution curves along k_y obtained from intensity spectra in Figs. 2B and 3B under circularly and linearly polarized MIR excitation, respectively. The blue curves are the ones passing through the Γ point. The green curves in (B) are through the avoided-crossing momenta. (**C**) EDCs through Γ under linearly (red squares) and circularly (blue circles) polarized pump at $t = 0$ fs, as well as the EDC through Γ taken at $t = -500$ fs (black).

The surface Dirac Hamiltonian hybridized with circularly polarized light essentially results in a Chern insulator as originally proposed by Haldane (*35*). In his model, alternating current loops break TRS locally, and the total magnetization remains zero. Whereas such microscopic periodic current configuration is difficult to implement, the Hamiltonian of graphene per valley in the Haldane model is basically the same as that of a circularly polarized electromagnetic field coupled to a Dirac band (*9*), which is realized in our experiment. These observations suggest the existence of a photoinduced anomalous quantum Hall phase without Landau levels where topological magnetoelectric effects described by axion electrodynamics may exist (*5*).

The quantitative agreement between the measured gap sizes and the models based on Floquet theory shows the general applicability of our result to Dirac systems. These observations open up an avenue for optical controlling and switching topological orders and may provide a platform for realizing Floquet Majorana modes in these materials (*1*, *2*).

References and Notes

1. M. Z. Hasan, C. L. Kane, *Rev. Mod. Phys.* **82**, 3045–3067 (2010).
2. X. L. Qi, S. C. Zhang, *Rev. Mod. Phys.* **83**, 1057–1110 (2011).
3. J. E. Moore, *Nature* **464**, 194–198 (2010).
4. C. Z. Chang *et al.*, *Science* **340**, 167–170 (2013).
5. X.-L. Qi, T. L. Hughs, S.-C. Zhang, *Phys. Rev. B* **78**, 195424 (2008).
6. Y. L. Chen *et al.*, *Science* **329**, 659–662 (2010).
7. S. Y. Xu *et al.*, *Nat. Phys.* **8**, 616–622 (2012).
8. H. Beidenkopf *et al.*, *Nat. Phys.* **7**, 939–943 (2011).
9. T. Kitagawa, T. Oka, A. Brataas, L. Fu, E. Demler, *Phys. Rev. B* **84**, 235108 (2011).
10. N. H. Lindner, G. Refael, V. Galitski, *Nat. Phys.* **7**, 490–495 (2011).
11. J. I. Inoue, A. Tanaka, *Phys. Rev. Lett.* **105**, 017401 (2010).
12. O. V. Yazyev, J. E. Moore, S. G. Louie, *Phys. Rev. Lett.* **105**, 266806 (2010).
13. C. Cohen-Tannoudji, J. Dupont-Roc, G. Grynberg, *Atom-Photon Interaction* (Wiley, Hoboken, NJ, 1992).
14. E. Goulielmakis *et al.*, *Nature* **466**, 739–743 (2010).
15. M. C. Rechtsman *et al.*, *Nature* **496**, 196–200 (2013).
16. F. M. Faisal, J. Z. Kaminski, *Phys. Rev. A* **56**, 748–762 (1997).
17. B. M. Fregoso, Y. H. Wang, N. Gedik, V. Galitski, http://arxiv.org/abs/1305.4145 (2013).
18. V. M. Galitskii, S. P. Goreslavskii, V. F. Elesin, *Sov. Phys. JETP* **30**, 117 (1970).
19. C. Kittel, *Introduction to Solid State Physics* (Wiley, Hoboken, NJ, 2004).
20. H. Sambe, *Phys. Rev. A* **7**, 2203–2213 (1973).
21. M. Schultze *et al.*, *Nature* **493**, 75–78 (2013).
22. Q. T. Vu *et al.*, *Phys. Rev. Lett.* **92**, 217403 (2004).
23. S. Ghimire *et al.*, *Nat. Phys.* **7**, 138–141 (2011).
24. G. Saathoff, L. Miaja-Avila, M. Aeschlimann, M. M. Murnane, H. C. Kapteyn, *Phys. Rev. A* **77**, 022903 (2008).
25. L. Miaja-Avila *et al.*, *Phys. Rev. A* **79**, 030901 (2009).
26. J. A. Sobota *et al.*, *Phys. Rev. Lett.* **108**, 117403 (2012).
27. M. Hajlaoui *et al.*, *Nano Lett.* **12**, 3532–3536 (2012).
28. Y. H. Wang *et al.*, *Phys. Rev. Lett.* **109**, 127401 (2012).
29. Y. H. Wang *et al.*, *Phys. Rev. Lett.* **107**, 207602 (2011).
30. A. D. LaForge *et al.*, *Phys. Rev. B* **81**, 125120 (2010).
31. Materials and methods are available as supplementary materials on *Science* Online.
32. S. V. Syzranov, M. V. Fistul, K. B. Efetov, *Phys. Rev. B* **78**, 045407 (2008).
33. Y. Zhou, M. W. Wu, *Phys. Rev. B* **83**, 245436 (2011).
34. T. Oka, H. Aoki, *Phys. Rev. B* **79**, 081406 (2009).
35. F. D. Haldane, *Phys. Rev. Lett.* **61**, 2015–2018 (1988).

Acknowledgments: This work is supported by U.S. Department of Energy (DOE) award numbers DE-FG02-08ER46521 and DE-SC0006423 (data acquisition and analysis) and Army Research Office (ARO-DURIP) grant W911NF-09-1-0170 (electron spectrometer). H.S. and P.J.-H. have been supported by the DOE, Basic Energy Sciences Office, Division of Materials Sciences and Engineering, under award DE-SC0006418 (materials growth). This work made use of the Materials Research Science and Engineering Center Shared Experimental Facilities supported by NSF under award DMR-0819762. We are grateful for the stimulating discussions with L. Fu, T. Kitagawa, T. Oka, B. Fregoso, and V. Galitski.

Supplementary Materials

www.sciencemag.org/content/342/6157/453/suppl/DC1
Materials and Methods
Supplementary Text
Figs. S1 to S4
References

30 April 2013; accepted 11 September 2013
10.1126/science.1239834

From Few to Many: Observing the Formation of a Fermi Sea One Atom at a Time

A. N. Wenz,[1,2]*† G. Zürn,[1,2]† S. Murmann,[1,2] I. Brouzos,[3] T. Lompe,[1,2,4] S. Jochim[1,2,4]

Knowing when a physical system has reached sufficient size for its macroscopic properties to be well described by many-body theory is difficult. We investigated the crossover from few- to many-body physics by studying quasi–one-dimensional systems of ultracold atoms consisting of a single impurity interacting with an increasing number of identical fermions. We measured the interaction energy of such a system as a function of the number of majority atoms for different strengths of the interparticle interaction. As we increased the number of majority atoms one by one, we observed fast convergence of the normalized interaction energy toward a many-body limit calculated for a single impurity immersed in a Fermi sea of majority particles.

The ability to connect the macroscopic properties of a many-body system to the microscopic physics of its individual constituent particles is one of the great achievements of physics. This connection is usually made using the assumption that the number of particles tends to infinity. Then a transition from discrete to continuous variables can be made, which greatly simplifies the theoretical description of large systems. When does a system become large enough for this approximation to be valid? This is a difficult question to answer because most calculations based on a microscopic description become prohibitively complex before their predictions approach the many-body solution. Experimentally, this question has been studied in the context of helium droplets (*1*) and nuclear physics (*2*) by measuring the emergence of superfluidity for increasing system size. We addressed this question with the use of ultracold lithium atoms, which have already been used to study few-particle systems with tunable interactions (*3*–*5*).

In our experiments, we control the system size on the single-particle level while maintaining full control over the interparticle interactions. We achieve this by deterministically preparing few-particle systems of ultracold ^{6}Li atoms (*6*) whose interparticle interaction can be tuned using Feshbach resonances (*7*, *8*). This allows us to explore the crossover from few- to many-body physics by studying the fermionic quantum impurity problem, where a single impurity atom interacts with a number of fermionic majority atoms. The majority atoms do not interact with each other because of the Pauli principle. In this system the impurity acts as a test particle, which we use to probe the majority component. The limit of a single majority particle (Fig. 1A) has been thoroughly

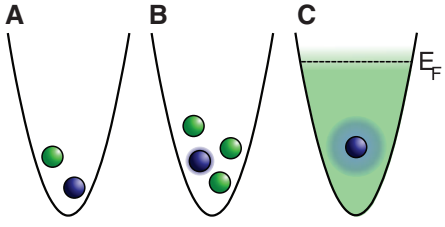

Fig. 1. From few to many. A single impurity (blue) interacting with one, few, and many fermions (green) in a harmonic trapping potential. In the many-body case, the majority component can be described as a Fermi sea with a Fermi energy E_F.

[1]Physikalisches Institut, Ruprecht-Karls-Universität Heidelberg, 69210 Heidelberg, Germany. [2]Max-Planck-Institut für Kernphysik, Saupfercheckweg 1, 69117 Heidelberg, Germany. [3]Institut für Quanten-Informationsverarbeitung, Universität Ulm, 89069 Ulm, Germany. [4]Extreme Matter Institute (EMMI), GSI Helmholtzzentrum für Schwerionenforschung, 64291 Darmstadt, Germany.

*Corresponding author. E-mail: wenz@physi.uni-heidelberg.de
†These authors contributed equally to this work.

Science

Observation of Floquet-Bloch States on the Surface of a Topological Insulator

Y. H. Wang, H. Steinberg, P. Jarillo-Herrero and N. Gedik

Science **342** (6157), 453-457.
DOI: 10.1126/science.1239834

Topological Replicas

When a periodic perturbation couples strongly to electrons in a solid, replicas of the original electronic levels are predicted to develop at certain energies—the so-called Floquet-Bloch states. Such conditions can be achieved by shining light on a solid, but the effect is challenging to observe. **Wang *et al.*** (p. 453) used time- and angle-resolved photoemission spectroscopy to photoexcite Bi_2Se_3 and observe its dispersion at various delay times. The replicas were seen at expected energy shifts, along with the gaps predicted to occur at the new energy-level crossings caused by the appearance of the replicas. Because Bi_2Se_3 is a topological insulator, the breaking of the time-reversal symmetry caused by circularly polarized light resulted in the appearance of an energy gap at the Dirac point, indicating an interesting route toward manipulating electronic states in such materials.